Li-ion battery anodes combining intercalation and plating energy storage mechanisms through SiO_x/C coated graphite

Ruhan He, Qiu He, Zhuo Chen, Rui Wang, Liang Zhou, Yeonguk Son, Liqiang Mai, Michael De Volder**

R. H. He, R. Wang, Prof. M. De Volder
Department of Engineering, University of Cambridge, 17 Charles Babbage Road, CB3 0FS Cambridge, UK.
E-mail: mfld2@cam.ac.uk (Prof. M. De Volder, ORCiD ID 0000-0003-1955-2270)

R. H. He, Z. Chen, Prof. L. Zhou, Prof. L. Q. Mai
State Key Laboratory of Advanced Technology for Materials Synthesis and Processing, Wuhan University of Technology, Luoshi Road 122, Wuhan 430070, Hubei, China
E-mail: mlq518@whut.edu.cn (Prof. L. Q. Mai, ORCiD ID 0000-0003-4259-7725)

Y. Son
Department of Chemical Engineering, Changwon National University, Changwon, Gyeongsangnam-do 51140, Republic of Korea

Prof. M. De Volder
The Faraday Institution, Quad One, Harwell Science and Innovation Campus, Didcot, UK

Q. He,
College of Materials Science and Engineering, Sichuan University, Chengdu 610065, China

Keywords: hybrid anode, lithium intercalation, lithium plating, graphite, lithiophilic coating

Abstract

Anode-less batteries are one of the most promising technologies to increase the energy density of lithium-ion batteries (LIBs). However, compared to conventional LIBs with graphite anodes, they tend to degrade much more rapidly. To balance energy density and lifetime, we propose a hybrid anode where part of the energy is stored by the lithiation of graphite and part by plating Li on graphite. Without special measures, the latter leads to accelerated capacity loss, which we address here by coating the graphite with a thin lithiophilic SiO_x/C layer using a scalable sol-gel process. By tuning the thickness of the SiO_x/C layer and modifying a localized high concentration electrolyte, we achieved a long-term balance in hybrid anodes, simultaneously realizing a highly

reversible Li plating/stripping while preserving high-capacity contribution from graphite intercalation with a considerable Li plating contribution (1/3). Overall, this results in hybrid anodes with a specific capacity of 584 mAh g^{-1} and capacity retention of 86 % over 500 cycles in a full cell versus NMC532 with an N/P ratio of 0.67. This far exceeds the 372 mAh/g theoretical capacity of graphite while at the same time doubling the lifetime compared to the best anode-less batteries reported to far.

Introduction

As the energy density of lithium-ion batteries (LIBs) with graphite anodes are approaching their theoretical limits, new anode concepts are being developed.[1], [2] Ultimately, anode-less batteries offer the highest possible energy density where, instead of inserting Li^+ in an anode host material during charging, it is instead plated as Li metal onto a Cu current collector. This approach allows for a simple anode manufacturing process (i.e. only a Cu foil), and unmatched energy density due to Li's extremely low redox potential (-3.04 V vs SHE) and ultra-high theoretical specific capacity (3862 mAh g^{-1}). Unfortunately, anode-less batteries suffer from rapid capacity fade, mainly due to rapid Li inventory loss caused by processes such as "dead Li" formation and unstable solid electrolyte interfaces (SEI).[2], [3], [4] Recently, a few research groups, including our own, have proposed to balance the anode capacity and lifetime by designing electrodes where part of the capacity is stored by graphite intercalation or silicon alloying and part by Li plating. [5], [6], [7] One way to think of this system is a standard battery with an N/P ratio < 1, where excess Li is plated on the anode once the graphite is fully intercalated. This approach is particularly attractive as it relies on well-established graphite anode manufacturing processes without the need to process Li-metal anodes or other reactive new anode chemistries. Furthermore, even after calendaring, graphite anodes retain sufficient porosity to accommodate substantial Li plating, [6, 8] and therefore there is no need to sacrifice the anode porosity for the proposed energy storage mechanism.

Unfortunately, practical realization of hybrid anodes still faces critical bottlenecks. First, the different orientations of commercial graphite, such as the edge plane or basal

plane, can induce uneven Li plating, making graphite a non-ideal substrate for lithium deposition.[9] The nonuniform plated Li tends to evolve into Li dendrites and "dead Li" depending on the cycling conditions, leading to fast capacity decay.[10], [11] Second, it remains challenging to achieve a balance between Li^+ intercalation and Li plating when these two processes exhibit close equilibrium potentials (last lithiation stage of Gr is around 0.07 V vs Li^+/Li) and share the same reaction interface. Due to this potential overlap, the hybrid electrode becomes increasingly vulnerable to Li plating especially when the deposited Li fraction grows.[12], [13] Although researchers have proposed coating graphite with Ag to prevent dendrite formation at high charging rates[14] or with Si to store Li by alloying reactions and to facilitate Li plating as an additional energy storage mechanism, there are several critical issues still need to be resolved.[6], [15], [16] It mainly includes two points: (1) certain Gr coatings are expensive and poorly scalable and (2) current electrolytes are not designed to simultaneously support stable Gr intercalation and Li metal plating, leading to poor performance in hybrid anode systems.

In this work we develop a scalable way to coat the surface of graphite with a hybrid material coating for reversible Li plating and stripping using a scalable wet chemistry process. Previously proposed methods such as Si chemical vapor deposition (CVD) and atomic layer deposition (ALD) coating used specialized equipment and are typically limited in throughput. Instead, we developed a conformal and lithiophilic biphasic SiO_x/C coating on the surface of graphite by a sol-gel process. The SiO_x/C coating, although only tens of nanometers in thickness, regulates the Li plating effectively and provides some charge capacity of its own. Second, the electrolytes proposed for these systems so far are designed for compatibility with Gr intercalation or Li plating. By optimising the coating thickness, and electrolytes that support both energy storage mechanisms, we achieve an overall capacity of 584 mAh g^{-1} in half cell and demonstrate full cell cycling against NMC532 (N/P=0.67; areal capacity > 2mAh/cm^2) with a capacity retention of 86 % over 500 cycles. This represents a substantial improvement over reference cells using uncoated graphite, whose capacity retention drops to 68 % after 200 cycles under the same conditions.

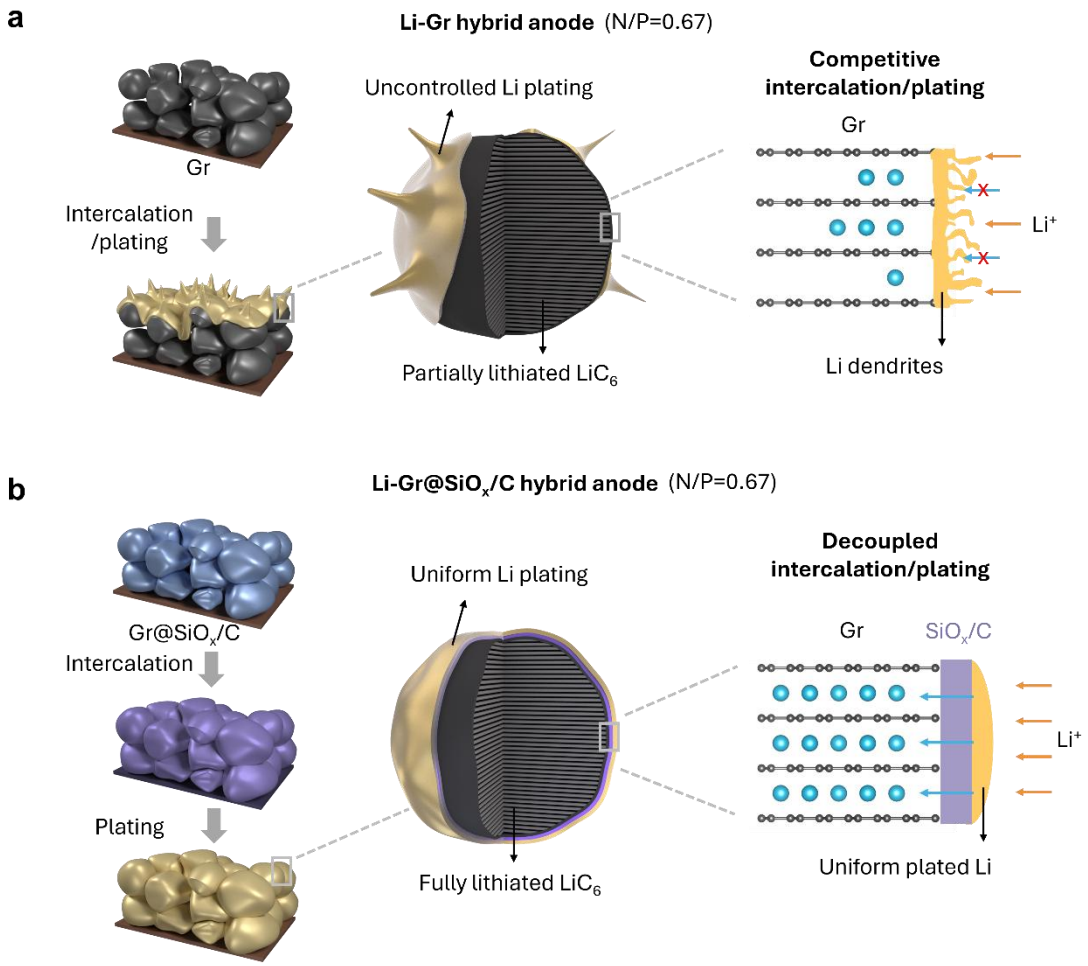


Figure 1 *Schematics of the proposed hybrid anode concept with combined intercalation and plating mechanisms. Illustration of Li plating on (a) Gr and (b) on Gr@SiO_x/C.*

Results and Discussion

Figure S1 shows a SEM picture of the artificial graphite starting material used in this study. Following the process depicted in Figure 2a, it is decorated with a conformal biphasic SiO_x/C layer, aimed to improve the lithium plating reversibility (Figure 1). The modification of the SiO_x/C layer is carried out through a two-step method (Figure 2a). The first step is the hydrolysation and condensation of vinyltrimethoxysilane (VTMS) or vinyltriethoxysilane (VTES) under Stöber reaction condition (water-ethanol-ammonia).[17] Under regular volumetric water/ethanol (5/2) ratio, spherical polyvinylsilsesquioxane (PVSQ) nanoparticles is formed in solution (i.e. homogeneous nucleation, Figure S2). By increasing the volume of ethanol, the reaction rate could be decreased, leading to the formation of a conformal PVSQ layer on the surface of

graphite (i.e. heterogeneous nucleation). The PVSQ polymer layer is transformed into a composite SiO_x/C nanolayer through annealing at 1000 °C under He flow (Figure 2b-2c). The weight ratio of SiO_x/C to Gr@SiO_x/C is tuned from 21.5% to 2.4% by controlling the volume of VTMS/VTES precursor (Table S1, Figure S3). The pristine graphite is denoted as 'Gr' and SiO_x/C coated graphite is denoted as 'Gr@SiO_x/C-*y*' with *y* referring to the weight ratio of SiO_x/C in Gr@SiO_x/C.

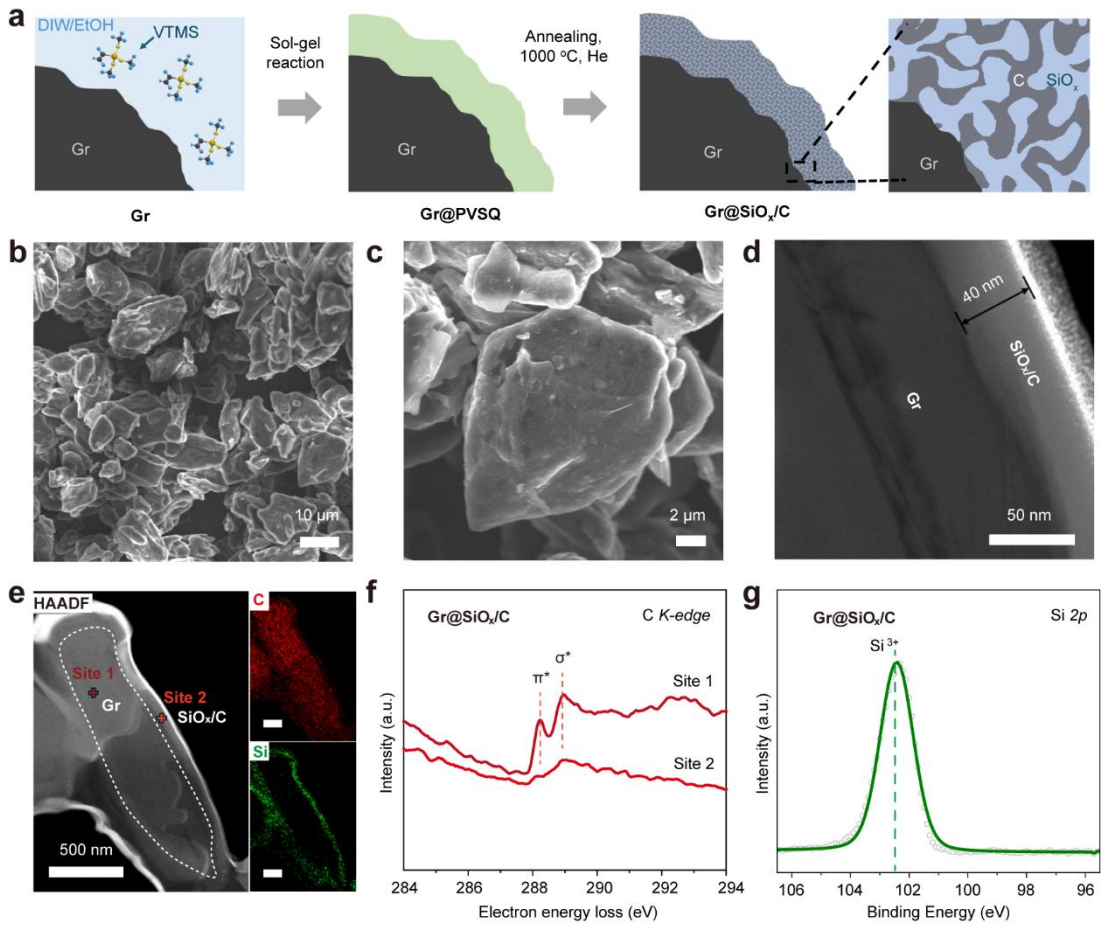


Figure 2 Characterizations of Gr@SiO_x/C. *(a) Schematic illustration of the SiO_x/C coating process on graphite particles. (b-c) Scanning electron microscopy (SEM) images of graphite after SiO_x/C coating (Gr@SiO_x/C). (d) Transmission electron microscopy (TEM) of a Gr@SiO_x/C lamella. (e) High-angle annular dark field-scanning transmission electron microscopy (HAADF-STEM) image of a lamella from a Gr@SiO_x/C particle and the corresponding elemental energy-dispersive spectroscopy (EDS) mapping images. The cross-sectional structure of the particle reveals a uniform SiOx/C coating layer around the Gr particle. (f) C K-edge electron energy loss*

spectroscopy (EELS) spectra of Gr@SiO_x/C from site 1 and site 2 pointed in (e). (g) High-resolution Si 2p XPS spectrum of Gr@SiO_x/C.

Diverse analytical tools were applied to verify the structure and compositions of Gr@SiO_x/C-*y*. As is shown in Figure S1 and S3, the morphology of the Gr and Gr@SiO_x/C-2.4% appears to show no significant differences in SEM micrographs. However, EDS mapping images reveal that the graphite particles was covered by a layer containing Si (Figure S4). The thickness of SiO_x/C layer for Gr@SiO_x/C-2.4% was measured to be 40 nm (Figure 2d). The HAADF-STEM image, along with the corresponding EDS mapping, indicated a rather uniform encapsulation of the graphite surface by the SiO_x/C layer (Figure 2e). It was difficult to distinguish the signal from the graphite bulk and from that of the carbon of SiO_x/C coating layer by Raman spectroscopy due to the strong signal from the carbon in the Gr substrate. In the carbon K-edge range in EELS spectra (Figure 2f), sharp σ* (~293 eV) and π* (~286 eV) peaks were clearly observed in the particle bulk, indicating a high degree of graphitization. However, only two broad carbon peaks were observed in the SiO_x/C coating, indicating that the SiO_x were surrounded by amorphous carbon. The XPS spectra confirmed the presence of Si in the coating with a Si valance of 3.0 (Figure 2g)[17]. According to the FTIR spectrum in Figure S5, the absorption bands located at 1226 cm^{-1} and 834 cm^{-1} from the Gr@SiO_x/C sample can be attributed to the stretching vibrations of Si-O-Si and Si-O bonds, respectively, which confirm the presence of partially oxidized silicon species within the composite. In this work, we study a bi-phasic coating layer combines amorphous carbon with SiO_x, because it offers better electronic conductivity and less volume expansion compared to pure Si, SiO_2. Further our wet-chemistry approach does not require large capital investment such as in the case of ALD or CVD based approaches.[18] The particle-size distributions from SEM images are compiled as statistical histograms in Figure S6. Gr@SiO_x/C-2.4% shows a mean particle size comparable to pristine graphite, consistent with a thin coating. As the weight ratio of SiO_x/C increases, the mean particle size shifts to larger value, indicative of thicker coating layer.

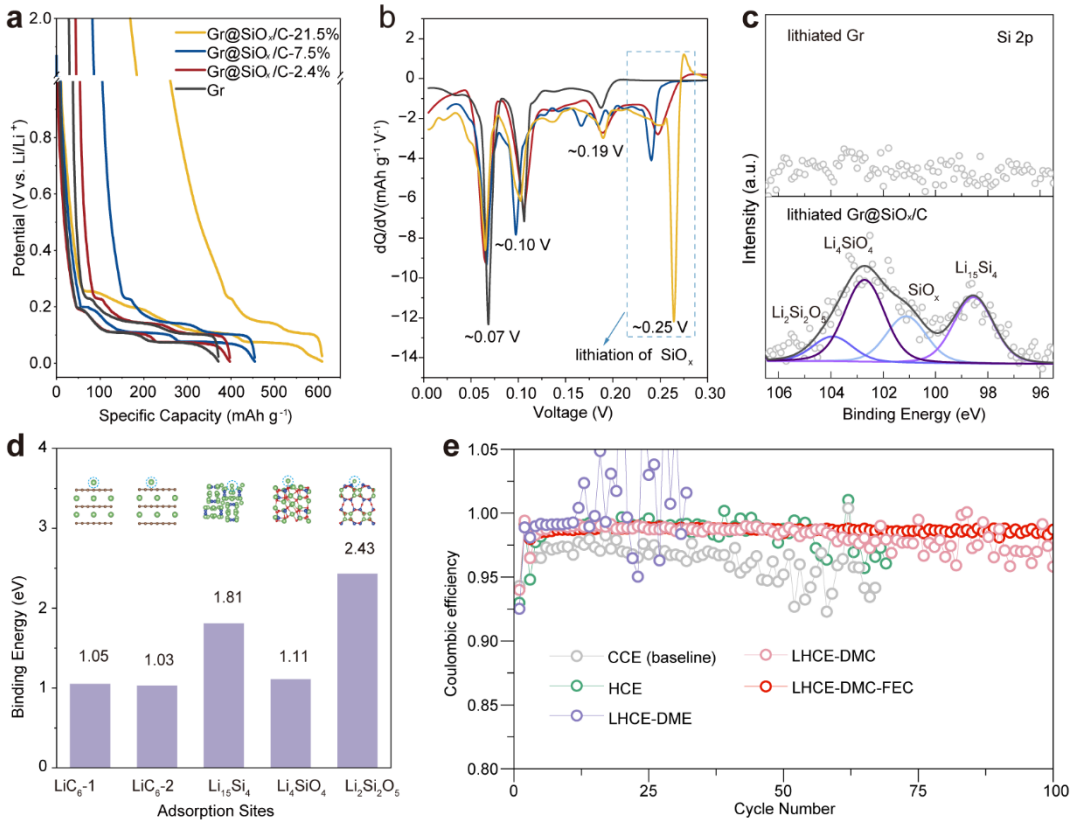


Figure 3 Analysis of *the Gr@SiO$_x$/C lithiation.* *(a) Galvanostatic voltage profiles and (b) the dQ/dV vs V curves of Gr and Gr@SiO$_x$/C-y (y = 21.5%, 7.5%, 2.4%) in the 1st cycle (0.005-2.0 V) at 0.1C. In this work, the C-rate was uniformly defined on a mass basis (1C = 371 mA g^{-1}, based on the theoretical capacity of graphite), so that all electrodes were tested under the same applied current density. (c) High-resolution Si 2p XPS spectrum of lithiated Gr and lithiated Gr@SiO$_x$/C. (d) Binding energies of Li$^+$ on the LiC$_6$ (001)-1, LiC$_6$ (001)-2, Li$_{15}$Si$_4$ (001), Li$_4$SiO$_4$ (10$\bar{3}$) and Li$_2$Si$_2$O$_5$ (010) with front views of the corresponding optimized structures. (e) Coulombic efficiencies of Gr@SiO$_x$/C-2.4%||Li half cells at 0.3 C in various electrolytes (1C corresponds to a current density of 600 mA g^{-1}).*

Next, we compared the specific capacities of Gr and Gr@SiO$_x$/C anodes between 0.005-2.0 V (i.e. without Li plating processes) for different weight ratios of SiO$_x$/C to Gr (Figure 3a, Table S1). As is shown in Figure S7 and Figure 3b, the additional reduction peaks at around 0.25 V correspond to the conversion reaction between Li$^+$ and SiO$_x$, which occurred prior to the Li$^+$ intercalation process of Gr (0.19 V, 0.10 V,

0.07 V).[19] As evidenced by Si 2p XPS spectrum in Figure 3c, the lithiation of Gr@SiO_x/C formed Li_xSi ($Li_{15}Si_4$ when it is fully lithiated) and lithium silicates (Li_4SiO_4 and $Li_2Si_2O_5$, which are denoted as Li-Si-O in the following parts) in addition to Li_xC[18]. Among all Gr@SiO_x/C-y samples, the Gr@SiO_x/C-2.4% electrode exhibited the highest initial Coulombic efficiency (ICE) of 89.0 % as well as the highest average CE (99.6 %) (Table S2) due to limited capacity stored in SiO_x (more cycling data is provided in Figure S7-S8).

The binding energies between lithium atoms and various nucleation sites on Gr and Gr@SiO_x were calculated to evaluate the Li affinity properties. The optimized structures included single Li atom binding with the LiC_6 (001)-1 (site 1), LiC_6 (001)-2 (site 2), $Li_{15}Si_4$ (001), Li_4SiO_4 ($10\bar{3}$) and $Li_2Si_2O_5$ (010), respectively (Figure 3e, Figure S9-S11). The results indicate that $Li_{15}Si_4$, Li_4SiO_4, and $Li_2Si_2O_5$ exhibit higher binding energy towards lithium than LiC_6. Materials with higher binding energies have been described in literature to promote more uniform nucleation and mitigate the risk of irregular lithium dendrite growth.[20]

We initially tested the proposed combination of lithiation and Li plating on Gr and Gr@SiO_x/C-2.4% in half-cells. In this cycling protocol, the anode is lithiated to a specific capacity of 600 mAh g^{-1} at a current density of 0.3 C (or 180 mA g^{-1}) and is subsequently de-lithiated to an upper cut-off voltage of 2.0 V. Carbonate solvent-based electrolytes (CCE) are known to be sub-optimal for Li plating processes. Here, the coulombic efficiency of cells using CCE drops to 95% after only 50 cycles when applied in hybrid anode system (Figure 3e). Therefore, we tested electrolytes that are known to operate better for lithium metal or anode-less batteries (Figure 3e, Figure S12, Table S3). [13], [21], [22] The results demonstrate that the localized high concentration electrolytes with the modification of FEC, LHCE-DMC-FEC (1.4 M LiFSI in DMC/EC/BTFE (25/1/40, v/v) + 5 wt % FEC) enable the hybrid anode to achieve better cycling stability than carbonate-based electrolyte.

When using LHCE-DMC-FEC electrolyte, the galvanostatic voltage profiles of Gr@SiO_x/C-2.4% electrode during the lithiation process (Figure 4a) clearly show the hybrid Li storage processes: In the region AB in Figure 4a, the Li^+ conversion reaction

with SiO_x and the Li^+ intercalation into Gr (> 0 V) takes place; In the BC region, the Li plating on the electrode (< 0 V) occurs. [23], [24] The discharge capacity of the Gr@SiO_x/C-2.4% above 0 V is 355 mAh g^{-1} in the 1st cycle (AB region in Figure 4a), which means that when the battery is charged to 600 mAh g^{-1} it relies for more than one third on Li plating for energy storage. In comparison, if we carry out the same process on standard Gr anodes with no coating, we observe a slightly lower specific capacity of 335 mAh g^{-1} in the AB region (see Figure 4b), further the Li nucleation overpotential is higher (11 mV on Gr versus 6 mV on Gr@SiO_x/C, see Figure 4a-4b, Figure S13). The Gr@SiO_x/C-2.4% electrodes also show a lower overpotential between the Li plating and the Li stripping process of 17 mV versus 28 mV for Gr electrodes. Importantly, after 50 cycles, the Gr@SiO_x/C electrodes maintain a similar capacity in the A'B' region whereas in contrast, the Gr electrode show a rapid decay of the energy stored in graphite down to 245 mAh·g^{-1} (A'B' region in Figure 4b).

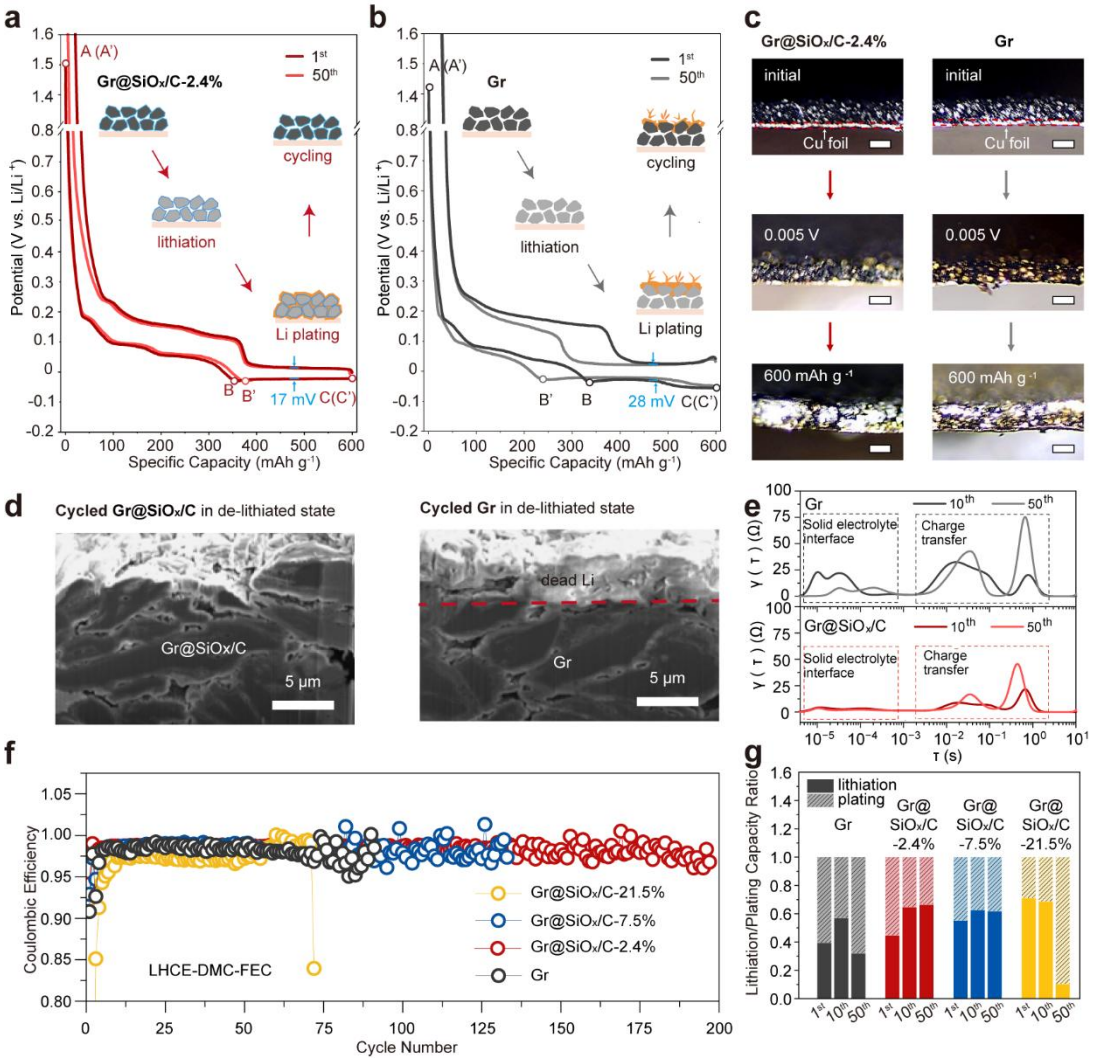


Figure 4 ***Electrochemical properties of Gr and Gr@SiO$_x$/C half-cells.*** *Galvanostatic voltage profiles of (a) Gr@SiO$_x$/C-2.4% and (b) Gr in the 1st and 50th cycle (after the formation cycles, discharged to 600 mAh g^{-1}). (c) Optical microscopy images of Gr@SiO$_x$/C-2.4% and Gr electrode at different lithiation state (initial, 0.005 V, 600 mAh g^{-1}), scale bar: 50 μm. (d) Gr@SiO$_x$/C-2.4% (left image) and Gr (right image) electrodes after cycling (in the de-lithiated state, charged to 2.0 V) after 50 cycles. (e) DRT analysis of the Nyquist plots of the Gr and Gr@SiO$_x$/C-2.4% electrodes after the 10th and 50th cycles. (f) The CE of Gr and Gr@SiO$_x$/C-y anodes at 0.3 C in LHCE-DMC-FEC electrolyte at 600 mAh g^{-1} (g) The ratio of the total capacity contributed by lithiation and Li plating in the 1st, 10th and 50th cycles.*

We applied optical microscopy to observe the electrodes during the charging

process (Figure 4c). The acquisition protocol of images in Figure 4c was illustrated in Figure S14. For Gr@SiO_x/C electrode, the electrode color changed from black in the delithiated state to a widespread light golden when charged to 0.005 V. When it was further charged to 600 mAh g^{-1}, the silver-colored lithium metal spreads across the Gr@SiO_x/C electrode cross-section. However, in the case of uncoated Gr electrodes, metallic lithium mainly accumulated on the upper parts of the electrode, while the lower part remained golden yellow. These results demonstrate the role of SiO_x/C in distributing the Li plating across the electrode.

The hybrid lithium storage behavior of Gr and Gr@SiO_x/C anodes was further characterized by SEM after cycling for 10 times. Cross-sectional SEM images of de-lithiated cells in Figure 4d confirm that Gr electrodes covered with a layer that is probably a combination of SEI and "dead Li" that contributes to capacity loss in the cell. On the other hand, the Gr@SiO_x electrode shows a much thinner layer on the surface with no obvious signs of dead lithium formation. Electrochemical impedance spectroscopy (EIS) was conducted in half cells at 80 % SOC (Figure S15) and are converted to relaxation-based function $\gamma(\tau)$ using dynamic relaxation time (DRT) analysis (Figure 4e).[25], [26], [27] This shows that the $\gamma(\tau)$ associated with the SEI is lower for Gr@SiO_x/C-2.4% electrodes compared to uncoated Gr. Further, the charge transfer resistance (R_{ct}) of Gr@SiO_x/C-2.4% electrode remains relatively stable ($R_{ct\text{-}10th}$ = 14.5 Ω, $R_{ct\text{-}50th}$ = 20.1 Ω) whereas in the case of bare Gr, we observe a twofold increase in the charge-transfer resistance ($R_{ct\text{-}10th}$ = 20.4 Ω, $R_{ct\text{-}50th}$ = 47.30 Ω). This could be due to excessive formation of SEI and/or "dead Li" on the top of bare Gr layer.[6]

The Coulombic efficiency (CE) and the specific capacity of hybrid anode in half cells during cycling was evaluated in Figure 4f and Figure S16. It shows that Gr@SiO_x/C-2.4% exhibits better cycling stability than pristine Gr when using LHCE-DMC-EC/FEC electrolyte.[21], [13] Even in the optimized electrolyte, pristine Gr exhibits pronounced Coulombic-efficiency decay after ~75 cycles, together with larger capacity fluctuations and faster fading, whereas Gr@SiO_x/C-2.4% maintains much higher Coulombic efficiency and more stable capacity retention (Figure 4f and Figure S16-S17). This contrast demonstrates that an appropriately uniform coating is essential for

forming a robust passivating interphase, regulating Li plating, and enabling long-term cycling stability. Gr@SiO_x/C-2.4% exhibits a Li plating reversibility of 99.0%, where Li plating contributes 33 % of total capacity of 600 mAh g^{-1}. In addition, the Gr@SiO_x/C-2.4% with thin coating outperform the Gr@SiO_x/C-21.5% thicker coatings in cycling stability. The trends are summarized in the histograms of Figure 4g that capture the evolution of the ratio of capacity stored in the lithiation of Gr (and SiO_x). This figure also shows the effect of increasing the weight ratio of SiO_x/C to Gr from 2.4% to 7.5% and 21.5%. The higher the SiO_x content, the lower the initial reliance on Li plating, which is due to SiO_x's higher specific capacity than Gr. However, after 50 cycles, Gr@SiO_x/C-2.4% is the only sample that maintained a high-capacity contributions from Gr intercalation (Figure 4g and Figure S18). This might be due to stresses at the interface of the Gr and SiO_x due to the volume expansion of thicker coatings. In agreement with Figure 4f, this confirms the importance of retaining a high-capacity retention in Gr@SiO_x/C and limiting the capacity contribution from the less stable lithium plating process.

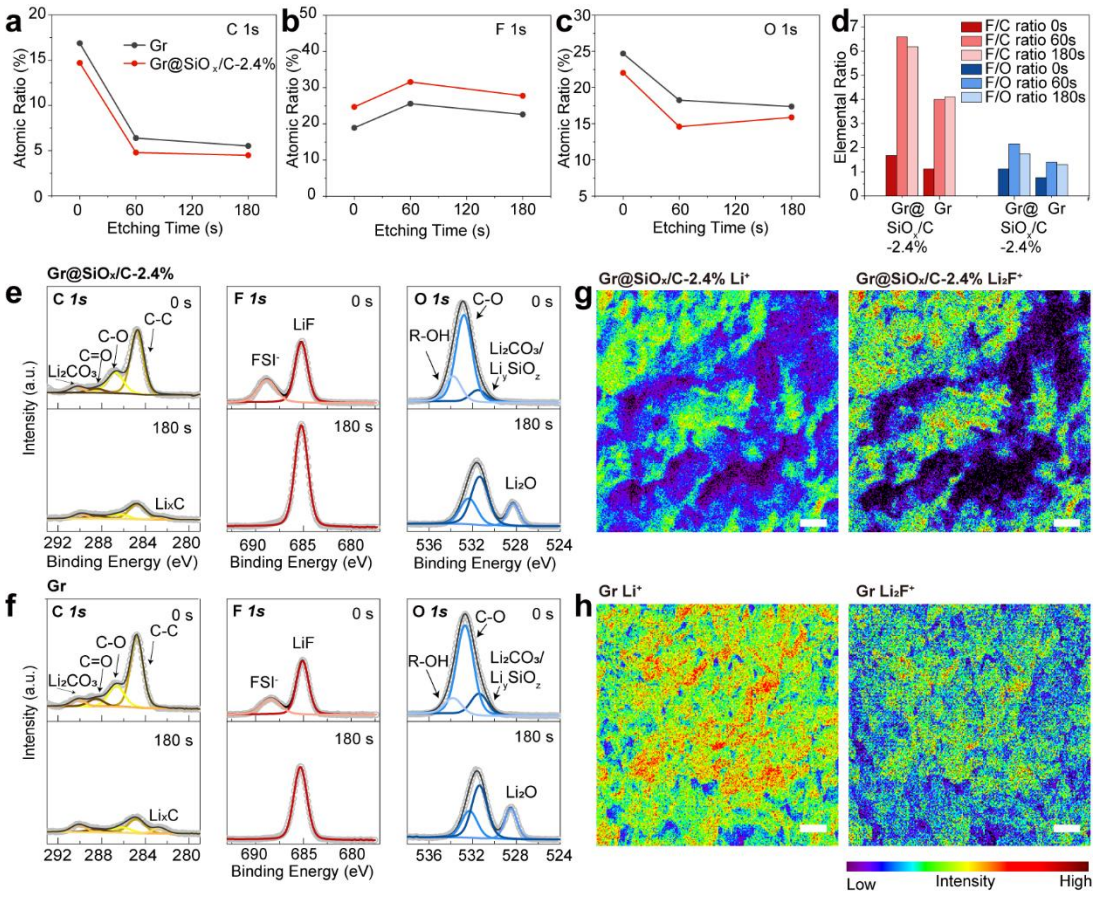


Figure 5 ***Characterization of interfacial chemical components on cycled Gr and Gr@SiO$_x$ hybrid electrodes.*** *Quantified (a) F, (b) C, (c) O atomic ratios, (d) F/C and F/O ratio of the XPS spectra obtained from Gr and Gr@SiO$_x$-2.4% (before etching, after 60s etching and after 180s etching). C 1s, F 1s, and O 1s XPS spectra obtained from (e) Gr@SiO$_x$-2.4% and (f) Gr (before etching and after 180s etching). TOF-SIMS mapping images of Li^+ and Li_2F^+ ions (clusters) from (g) Gr@SiO$_x$-2.4%, (h) Gr electrodes. All the electrodes mentioned above were cycled in LHCE electrolyte 10 times in half-cells (scale bar: 10 μm).*

Depth-profiling XPS analysis was employed to investigate the SEI composition on Gr, Gr@SiO$_x$/C-2.4% and Gr@SiO$_x$/C-21.5% electrodes after the first lithiation and after 10 cycles. The atomic ratios of the F, C, O, F/C and F/O elements and their regional spectra are shown in Figure 5a-5f and Figure S19-S20. (1) The SEI of Gr@SiO$_x$/C-2.4% exhibit notably lower C (carbon) levels (14.7 %) yet higher F, S, and N contents compared to the SEI of Gr and Gr@SiO$_x$/C-21.5% (Figure S19), suggesting increased inorganic content (LiF, Li_2S, Li_3N) (Figure 5a-5c). This is also verified by the strong intensity of LiF in the F *1s* spectra of Gr@SiO$_x$/C-2.4% shown in Figure 5e. (2) The ratio of F content increases rapidly within the first 60 s of sputtering and remains at a high level (27.8 %) after 180 s sputtering, while C decreases to only 4.5 % after 180 s sputtering (Figure 5a-5b), suggesting a high F/C ratio at the base of the SEI (Figure 5d). This is further verified by the enhanced intensity of LiF in F *1s* spectra along with a substantial reduction of the organic species signals (C-C, COR (R: radicals), HCO_2Li/COOR) in C *1s* spectra with 180 s sputtering (Figure 5e). These results reveal a compositional gradient from an organic-rich exterior to a LiF-rich interior for SEIs formed on Gr@SiO$_x$/C-2.4%. LiF-rich SEIs are often reported to be beneficial for Li-metal anodes [28], [29], which agree with the observations in this work. Uncoated Gr electrode exhibits similar compositional gradients, but with a notably lower F ratio (22.6 %) and lower F/C ratio, which is also indicated by the decreased intensity of LiF peaks in the high resolution F1s XPS spectra (Figure 5f). However, the inner layer contains more Li-O species forms (Figure S20a).

Next, we further investigated the interfacial evolution of Gr and Gr@SiO_x/C SEI in the de-lithiated state after 10 cycles using time of flight-secondary ion mass spectrometry (TOF-SIMS). The analysis shows that Gr@SiO_x/C-2.4% (Figure 5g) electrodes have less Li residues on their surface than Gr and Gr@SiO_x/C-21.5% electrodes (Figure 5h, S20b), with the former showing stronger Li_2F^+ signals, in agreement with the higher LiF content observed by XPS. In addition, the amount of dead lithium generated on Gr@SiO_x/C-2.4% is lower than that of pristine Gr and Gr@SiO_x/C-21.5%. These results demonstrate that the SiO_x coating and its thickness plays an important role in the composition of the SEI.[30] Galvanostatic intermittent titration technique (GITT, Figure S21) tests after 10 cycles suggest that Gr@SiO_x/C exhibits a slightly higher average D_{Li}^+ value (6.56×10^{-10} cm^2 S^{-1}) than Gr (5.76×10^{-11} cm^2 S^{-1}), suggesting that the SiO_x/C coating helps to improve the Li^+ interfacial kinetics as well. Further, electrochemical impedance spectroscopy (EIS) data was collected at different states of charge (SOC) (Figure S22). The R_{ct} of Gr@SiO_x/C decreases as the lithiation degree increased, but the R_{ct} of Gr increases at the initial lithiation stage and drops at the following stage.[26], [27]

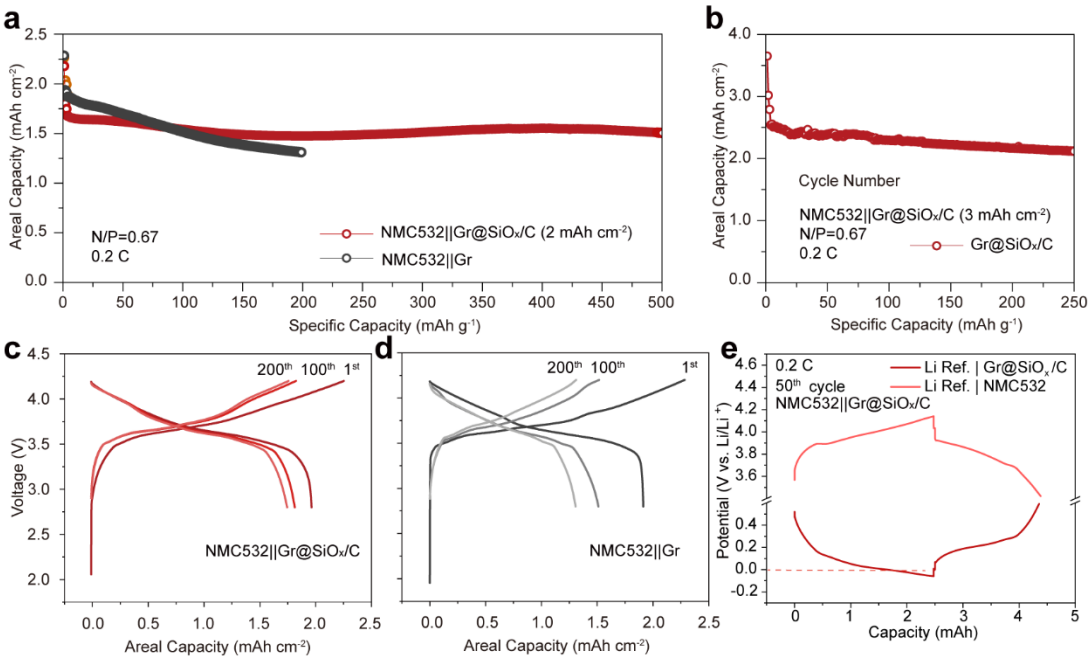


Figure 6 ***Electrochemical performance in full cells.*** *Cycling performance of full cells with N/P=0.67 paired with NMC532 with an areal capacity equaling to (a) 2 mAh* cm^{-2} *and (b) 3 mAh* cm^{-2}*. Galvanostatic voltage profiles at the 1st, 100th and 200th cycles of*

(c) NMC532||Gr@SiO_x/C and (d) NMC532||Gr full cells. (e) Voltage curves of the three-electrode NMC532||Gr@SiO_x/C cell using a Li metal reference electrode (Li Ref.).

Finally, the viability of our Li-Gr@SiO_x/C anodes for the proposed dual energy storage mechanism is verified using NMC532 cathodes with an N/P ratio of 0.67 (Figure 6a, Figure S23). In such cell design, one third of the capacity stored in an "anode-less" plating and stripping mode (charging full cells with a low N/P ratio corresponds to plating excessive cathodic Li inventory on the anode). The ICE of cells using Gr@SiO_x/C is 3.7 % lower than that of pure Gr, possibly due to irreversible SiO_x conversion reactions (Figure 6c-6d). However, in subsequent cycles the stability of Gr@SiO_x/C anodes far outperform Gr reaching 86 % capacity retention after 500 cycles (for NMC532 || Gr@SiO_x/C), versus 68% after 200 cycles (for NMC532 || Gr). To the best of our knowledge, the capacity retention in our work are among the highest than hybrid anodes and the anode-less reported under comparable conditions (verses NMC cathode; N/P < 1, areal capacity > 2 mAh cm^{-2}) (Figure S23-S25, Table S4-S5) [5, 6, 30]. If the areal capacity of NMC532 is further increased to 3 mAh cm^{-2} 71 % capacity is retained after 250 cycles (see Figure 6b and Figure S26). Voltage profiles of the SiO_x coated graphite at the 100^{th} and the 200^{th} cycle further show very little polarization build up in the cell (Figure 6c). On the other hand, polarization is noticeable when using pristine Gr anodes (Figure 6d), which in agreement with the above observations of thick layers of degradation products and the impedance spectroscopy. Voltage - capacity profiles of Gr@SiO_x/C vs. Li measured in three-electrode cells (Figure 6e) reveal that the Gr@SiO_x/C anode remain 64.4 % of its capacity from Li intercalation and 35.6 % from Li plating after 50 cycles. In contrast, for the Gr||NMC532 full cell, after only 40 cycles, intercalation accounts for merely 18 % of the total charge capacity, with the majority originating from Li plating with a large overpotential (23 mV) (Figure S27). This shows rapid capacity decay of Gr when Li is plated on it without appropriate coating, which is consistent with the trends identified earlier in half-cell studies. The porosity calculation results indicate that, under the same level of areal capacity (~ 2

mAh cm^{-2}), Gr@SiO_x/C and Gr exhibit comparable porosity before and after calendaring, whereas the Gr@SiO_x/C electrode is relatively thinner (Table S6). Therefore, the more uniform Li plating observed on Gr@SiO_x/C is more reasonably attributed to the lithiophilic SiO_x/C coating than a geometrical advantage arising from electrode thickness or pore volume. The results show that NMC532||Gr@SiO_x/C full cells exhibit high stability in terms of cycling with a practical areal capacity and demonstrates the potential benefits of balancing energy storage in anodes through different mechanisms.

Conclusion

Anode-less batteries are one of the most promising technologies to increase the energy density of Li-ion batteries. However, to date, the repeated Li metal plating and stripping taking place in these anodes lead to poor cycling stability. In this paper, we use a classic graphite anode as a scaffold for Li plating, which at the same time allows for stable energy storage by Li intercalation. Li plating and stripping on the surface of pristine Gr leads to the formation of excessive SEI and degradation of the Gr capacity. We developed a scalable sol-gel method for coating Gr with a combination of SiO_x and amorphous carbon. Paired with NMC532 cathodes and LHCE-DMC-FEC electrolyte, these Gr@SiO_x/C anodes achieve capacity retentions up to 86% over 500 cycles when storing one third of the capacity in Li metal plating. Importantly, this process relies on standard graphite anode processing methods and is therefore compatible with existing industrial capital equipment investments and large-scale manufacturing processes.

Data Availability

The data supporting this article are available from the corresponding author upon reasonable request.

Conflicts of interest

There are no conflicts to declare.

Acknowledgements

This work was supported by the European Research Council (ERC CoG MIGHTY - 866005) and the Faraday Institution Degradation Project (FIRG060).

References

[1] M. N. Obrovac, V. L. Chevrier, *Chem. Rev.* **2014**, 114, 11444.
[2] X.-B. Cheng, R. Zhang, C.-Z. Zhao, Q. Zhang, *Chem. Rev.* **2017**, 117, 10403.
[3] S. Nanda, A. Gupta, A. Manthiram, *Adv. Energy Mater.* **2021**, 11, 2000804.
[4] C.-J. Huang, B. Thirumalraj, H.-C. Tao, K. N. Shitaw, H. Sutiono, T. T. Hagos, T. T. Beyene, L.-M. Kuo, C.-C. Wang, S.-H. Wu, W.-N. Su, B. J. Hwang, *Nat. Commun.* **2021**, 12, 1452.
[5] C. Martin, M. Genovese, A. J. Louli, R. Weber, J. R. Dahn, *Joule* **2020**, 4, 1296.
[6] Y. Son, T. Lee, B. Wen, J. Ma, C. Jo, Y.-G. Cho, A. Boies, J. Cho, M. De Volder, *Energy Environ. Sci.* **2020**, 13, 3723.
[7] G. Park, S. Kim, J. Kim, S. Bae, Y. Heo, D. Park, H. Kim, J. Shin, J. Moon, J. W. Choi, *Adv. Energy Mater.* **2024**, 2401289.
[8] Y. Liu, X. Qin, F. Liu, B. Huang, S. Zhang, F. Kang, B. Li, *ACS Nano* **2020**, 14, 1837.
[9] M. Velický, P. S. Toth, C. R. Woods, K. S. Novoselov, R. A. W. Dryfe, *J. Phys. Chem. C* **2019**, 123, 11677.
[10] P. Arora, M. Doyle, R. E. White, *J. Electrochem. Soc.* **1999**, 146, 3543.
[11] T. Gao, Y. Han, D. Fraggedakis, S. Das, T. Zhou, C.-N. Yeh, S. Xu, W. C. Chueh, J. Li, M. Z. Bazant, *Joule* **2021**, 5, 393.
[12] A. S. Mijailovic, S. Waag-Swift, G. Wang, B. Zhou, M. Luo, W. Lu, Q. Wu, B. W. Sheldon, *Energy Environ. Sci.* **2024**, 17, 8702.
[13] W. Cai, C. Yan, Y.-X. Yao, L. Xu, X.-R. Chen, J.-Q. Huang, Q. Zhang, *Angew. Chem. Int. Ed.* **2021**, 60, 13007.
[14] H. Jia, J.-M. Kim, P. Gao, Y. Xu, M. H. Engelhard, B. E. Matthews, C. Wang, W. Xu, *Angew. Chem. Int. Ed.* **2023**, 62, e202218005.
[15] D. Lin, Y. Liu, Y. Cui, *Nat. Nanotechnol.* **2017**, 12, 194.
[16] R. He, Y. Wang, C. Zhang, Z. Liu, P. He, X. Hong, R. Yu, Y. Zhao, J. Wu, L. Zhou, *Adv. Energy Mater.* **2023**, 13, 2204075.
[17] Z. Liu, D. Guan, Q. Yu, L. Xu, Z. Zhuang, T. Zhu, D. Zhao, L. Zhou, L. Mai, *Energy Storage Mater.* **2018**, 13, 112.
[18] Z. Liu, Q. Yu, Y. Zhao, R. He, M. Xu, S. Feng, S. Li, L. Zhou, L. Mai, *Chem. Soc. Rev.* **2019**, 48, 285.
[19] X. Lu, M. Lagnoni, A. Bertei, S. Das, R. E. Owen, Q. Li, K. O'Regan, A. Wade, D. P. Finegan, E. Kendrick, M. Z. Bazant, D. J. L. Brett, P. R. Shearing, *Nat. Commun.* **2023**, 14, 5127.
[20] D. Lin, Y. Liu, Y. Cui, *Nat. Nanotechnol.* **2017**, 12, 194.
[21] C. Gervillié-Mouravieff, L. Ah, A. Liu, C.-J. Huang, Y. S. Meng, *ACS Energy Lett.* **2024**, 9, 1693.

[22] S. Chen, J. Zheng, D. Mei, K. S. Han, M. H. Engelhard, W. Zhao, W. Xu, J. Liu, J.-G. Zhang, *Adv. Mater.* **2018**, 30, 1706102.
[23] C. Wang, Y. Xie, Y. Huang, S. Zhou, H. Xie, H. Jin, H. Ji, *Angew. Chem. Int. Ed.* **2024**, 63, e202402301.
[24] H. Sun, G. Xin, T. Hu, M. Yu, D. Shao, X. Sun, J. Lian, *Nat. Commun.* **2014**, 5, 4526.
[25] M. Derakhshan, E. Sahraei, D. Soudbakhsh, *Cell Rep. Phys. Sci.* **2022**, 3, 101102.
[26] Y. X. Yao, N. Yao, X.-R. Zhou, Z.-H. Li, X.-Y. Yue, C. Yan, Q. Zhang, *Adv. Mater.* **2022**, 34, 2206448.
[27] Y. Lin, W. Hu, M. Ding, Y. Hu, Y. Peng, J. Liang, Y. Wei, A. Fu, J. Lin, Y. Yang, Adv. Energy Mater. 2024, 14, 2400894.
[28] Z. Cui, Z. Jia, D. Ruan, Q. Nian, J. Fan, S. Chen, Z. He, D. Wang, J. Jiang, J. Ma, X. Ou, S. Jiao, Q. Wang, X. Ren, *Nat. Commun.* **2024**, 15, 2033.
[29] S. Liu, X. Ji, N. Piao, J. Chen, N. Eidson, J. Xu, P. Wang, L. Chen, J. Zhang, T. Deng, S. Hou, T. Jin, H. Wan, J. Li, J. Tu, C. Wang, *Angew. Chem. Int. Ed.* **2021**, 60, 3661.
[30] Y. Dong, Y. Chen, X. Yue, Z. Liang, *Energy Environ. Sci.* **2024**, 17, 2500.